Contrast-enhanced photoacoustic tomography of human joints

Chao Tian[*,a,b], Rahul K. Keswani[*,c], Girish Gandikota[b],
Gus R. Rosania[†,c] and Xueding Wang[†,a,b]

[a] Department of Biomedical Engineering, University of Michigan, Ann Arbor, MI 48109
[b] Department of Radiology, University of Michigan, Ann Arbor, MI 48109
[c] Department of Pharmaceutical Sciences, College of Pharmacy, University of Michigan, Ann Arbor, MI 48109

ABSTRACT

Photoacoustic tomography (PAT) provides a unique tool to diagnose inflammatory arthritis. However, the specificity and sensitivity of PAT based on endogenous contrasts is limited. The development of contrast enhanced PAT imaging modalities in combination with small molecule contrast agents could lead to improvements in diagnosis and treatment of joint disease. Accordingly, we adapted and tested a PAT clinical imaging system for imaging the human joints, in combination with a novel PAT contrast agent derived from an FDA-approved small molecule drug. Imaging results based on a photoacoustic and ultrasound (PA/US) dual-modality system revealed that this contrast-enhanced PAT imaging system may offer additional information beyond single-modality PA or US imaging system, for the imaging, diagnosis and assessment of inflammatory arthritis.

Keywords: Photoacoustic tomography, inflammatory arthritis, macrophage-targeting, FDA-approved contrast agent, Clofazimine

1. INTRODUCTION

Arthritis is a leading cause of disability among adults in the U.S. and is associated with decreased work productivity, reduced quality of life, and high health-care costs [1, 2]. To facilitate disease diagnosis and early therapeutic interventions, the National Institute of Arthritis and Musculoskeletal and Skin Diseases (NIAMS) has called upon the scientific community to develop early detection technologies, such as medical imaging devices that can be used to visualize soft tissue structure and function in the joints [3, 4].

Combining strong optical contrast and high ultrasonic resolution in a single modality, the emerging photoacoustic tomography (PAT) technology provides a unique opportunity to overcome the limitations of pure optical imaging modalities [5-9], and is poised to exert a profound impact on the diagnosis and treatment of joint disorders [3, 10-13]. However, although label-free imaging based on endogenous tissue contrasts is desirable, functional imaging probes and contrast agents could drastically enhance the performance of PAT in terms of sensitivity, specificity, and the number of functional and molecular biomarkers. A state-of-the-art photoacoustic molecular imaging platform powered by advanced photoacoustic contrast agents can shift the paradigm of diagnosis and characterization of inflammatory conditions, and can contribute to better understanding the pathophysiology of diseases as well as their responses to pharmaceutical and non-pharmaceutical therapies [13, 14].

Here, we test whether combining photoacoustic (PA) imaging together with ultrasound (US) imaging may offer advantages as a contrast-enhanced PA/US imaging system, relative to US imaging or PA imaging modalities alone. For this purpose, we turned to an FDA-approved drug Clofazimine as a novel PAT contrast agent.

[*] Equal contribution
[†] Corresponding authors: grosania@umich.edu or xdwang@umich.edu

Photons Plus Ultrasound: Imaging and Sensing 2016, edited by Alexander A. Oraevsky, Lihong V. Wang
Proc. of SPIE Vol. 9708, 97084L · © 2016 SPIE · CCC code: 1605-7422/16/$18 · doi: 10.1117/12.2213749

Downloaded From: http://proceedings.spiedigitallibrary.org/ on 03/25/2016 Terms of Use: http://spiedigitallibrary.org/ss/TermsOfUse.aspx

2. MATERIALS AND METHODS

2.1 FDA-approved macrophage-targeting contrast agent Clofazimine

Clofazimine (CFZ) - $C_{27}H_{22}Cl_2N_4$, a poorly soluble, strongly pigmented R-imino phenazine antibiotic [Fig. 1(a)] [15-17]. It is a weak base with a pK_{a1} = 2.31 and pK_{a2} = 9.29 and is highly lipophilic (clog P ≈ 7). It has an extremely long retention time within tissues, and exhibits a long, highly variable pharmacokinetic half-life ($t_{1/2}$ ~ 70 days in humans, 7 days in mice) [18]. In aqueous solution, CFZ predictably exists in neutral, monoprotonated, and diprotonated states depending on the solution pH [Fig. 1(b)].

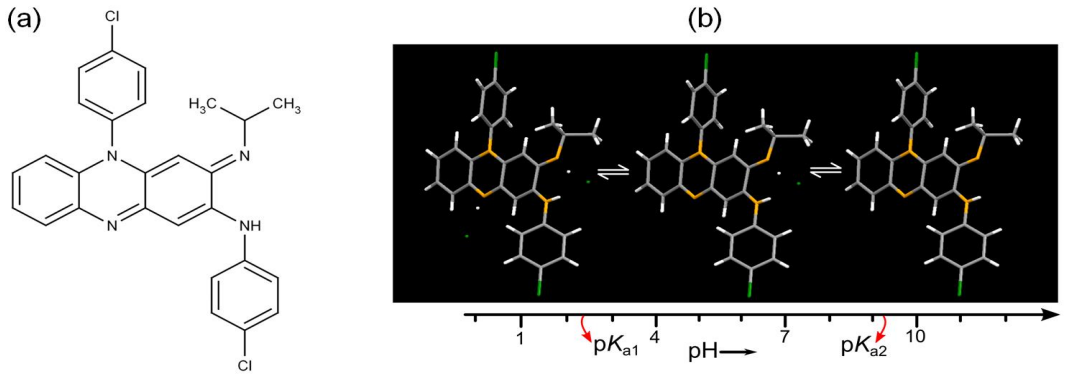

Fig. 1 CFZ (a) and its protonation states under different pH values (b). The figure is shown following simulation of chemical conditions via ChemAxon.

CFZ has little clinical toxicity [19, 20]. It is specifically beneficial as an anti-inflammatory agent for treating erythema nodosum [21, 22], the grossly disfiguring skin inflammation that afflicts leprosy patients. Interestingly, when administered orally for prolonged periods of time [23-25], CFZ massively accumulates in macrophages [26-28]. In these cells, it forms microscopic, red crystal-like drug inclusions (CLDIs) [26, 27, 29]. Since macrophages play a key role on inflammatory joint diseases, we see tremendous potential of CFZ as a macrophage-targeted photoacoustic contrast agent for the following reasons:

1) **FDA Approval**. As an orally bioavailable small molecule drug, CFZ is approved by the FDA for clinical use in humans [30, 31].
2) **Known Pharmacokinetics, Pharmacology and Toxicology in animals and humans**. CFZ has been the subject of extensive pharmacokinetics, pharmacological and toxicological studies in animals and human patients, since the 1970s [21, 26].
3) **Macrophage Targeting, Biocompatibility and Anti-Inflammatory Activity**. CFZ massively bioaccumulates in macrophages where it precipitates to form CLDIs [25-27, 29, 32]. Upon phagocytosis, CLDIs exert anti-inflammatory activity.
4) **Liposomal Encapsulation and Self-Assembly into Stable, Biocompatible Crystals**. CFZ has been formulated in a variety of different nanoparticle forms, including liposomal formulations. While liposomal encapsulation has been used to modulate the pharmacokinetics and decrease the toxicity of CFZ [33, 34], it can also be used to promote passive, macrophage-targeting [35, 36], and may provide a means to modulate biocompatibility, anti-inflammatory activity, and potentially, the photoacoustic properties of CFZ.
5) **Strong Visible Absorbance and Near IR Fluorescence Signals**. CFZ is red in color and fluoresces in the near infrared region of the electromagnetic spectrum, and its optical spectral properties are influenced by its protonation state and molecular configuration in the solid state [27, 29, 37].

2.2 PA/US dual-modality imaging system built on a commercial Verasonics ultrasound unit

The schematic of the photoacoustic and ultrasound (PA/US) dual-modality imaging system is shown in Fig. 2(a). The output laser (532 nm) is the second harmonic generation (SHG) output of the Nd:YAG (Powerlite DLS 8010, Continuum) laser with a pulse repetition frequency (PRF) of 10 Hz, pulse duration 6 ns and pulse energy greater than 800 mJ. The laser beam passes through a beam expander and illuminates on the finger joint, which excites ultrasound

Downloaded From: http://proceedings.spiedigitallibrary.org/ on 03/25/2016 Terms of Use: http://spiedigitallibrary.org/ss/TermsOfUse.aspx

signals. After being reflected by a glass slide, the excited ultrasound signals are received by a 128-element transducer array (L7-4 or CL15-7, Philips), transferred to the commercial Verasonics system (Vantage 256, Verasonics), reconstructed using a back-projection algorithm and finally displayed in real time. The system can acquire two-dimensional (2D) photoacoustic images at a frame rate of 10 Hz, which is only limited by the PRF of the laser. The calibrated spatial resolution of the PAT system was better than 300 μm in the imaged cross section [10].

Figure 2(b) shows a simple implementation of the image reconstruction process for a planar transducer based on the back-projection algorithm. When photoacoustic signals emits from the absorber, it takes different time of flight (TOF) for the signals to reach different elements of the transducer. For the *i*th unit of the array, the received photoacoustic signal could be from any point on a sphere centered at the *i*th unit and with a radius $R_i = v_s \times t_i$ (v_s: speed of sound, t_i: TOF to the *i*th unit). When all the 128 units are simultaneously taken into consideration, the intersection point can be located as the original photoacoustic source. 2D photoacoustic images can be finally reconstructed by a pixel-to-pixel back projection.

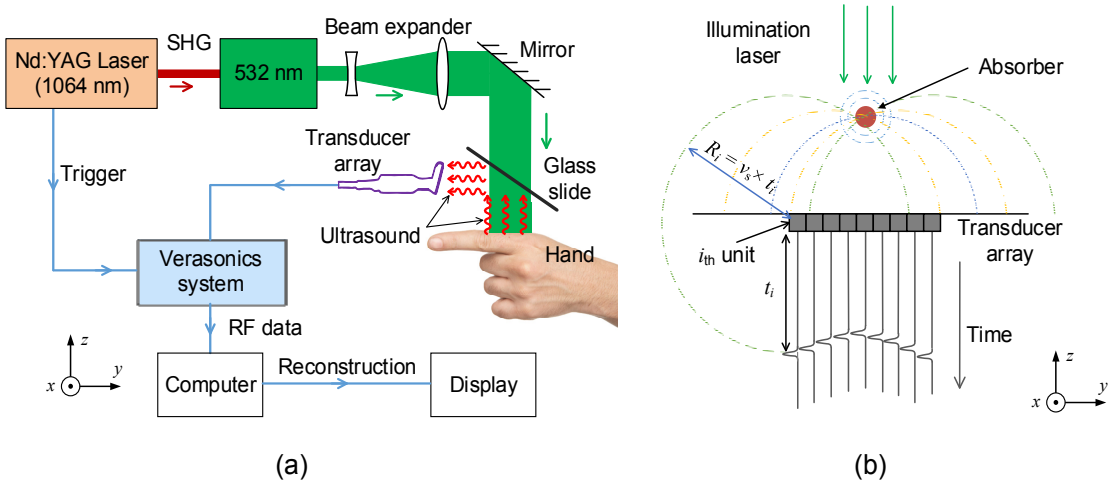

Fig. 2 Real-time PA/US dual-modality imaging system based on the commercial Verasonics unit. (a) System layout, (b) image reconstruction scheme from multi-channel RF signals. RF: radio-frequency, SHG: second-harmonic generation.

The US imaging functionality has been integrated with the PAT system through sequence programming of the Verasonics system and, therefore, PA/US dual-modality imaging can be achieved at the same time. During each cycle (0.1 s, limited by the PRF of the laser), the Verasonics system first works in the receiving mode to receive photoacoustic signals and then switches to the transmitting and receiving mode to perform US imaging. A function generator (3314A, Hewlett-Packard) was used to generate separate trigger signals for PA and US to ensure correct timing. Fig. 3 shows the physical setup of the integrated PA/US dual-modality imaging system.

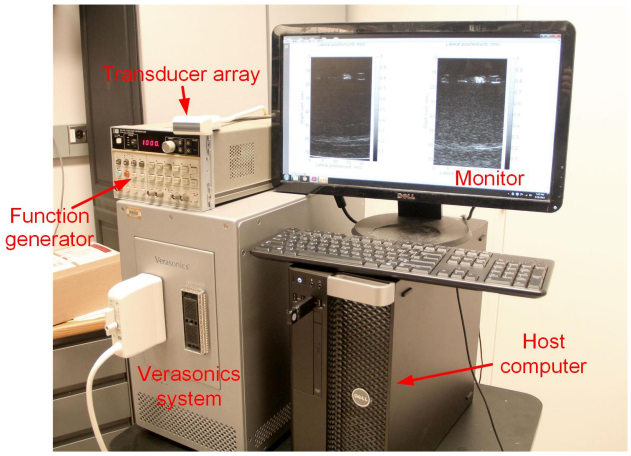

Fig. 3 Physical setup of the PA/US dual-modality imaging system

Downloaded From: http://proceedings.spiedigitallibrary.org/ on 03/25/2016 Terms of Use: http://spiedigitallibrary.org/ss/TermsOfUse.aspx

3. RESULTS

3.1 Chemical synthesis and analysis of different solid crystalline forms of CFZ

We synthesized crystalline solids by dissolving CFZ in MeOH and then adding an equal volume of 1M ammonium salts [29]. Fig. 4(a) shows that the resulting precipitates varied in color and morphology. Powder X-ray diffractograms (pXRDs) indicate differences in molecular organization of CFZ in the various solids [Fig. 4(b)]. CFZ crystals formed in acetate and carbonate buffer resulted in the precipitation of free base CFZ crystals (CFZ-TC). Proton nuclear magnetic resonance (^{1}H-NMR) spectra of dissolved crystals show CLDIs, Cl^-, Br^-, and I^- are composed of protonated CFZ salts, whereas the other crystals are solid polymorphs of CFZ free base [Fig. 4(c)].

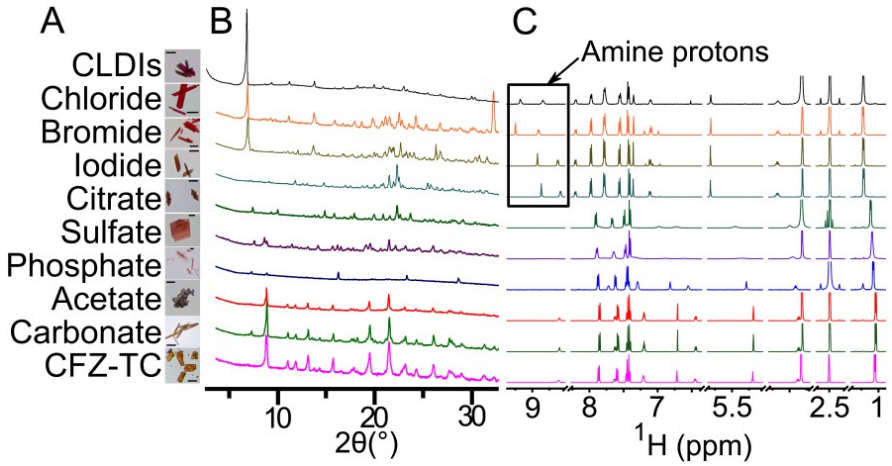

Fig. 4 Chemical synthesis and analysis of different solid crystalline forms of CFZ. (a) Color and morphology of different solid crystalline forms of CFZ; (b) pXRDs of different solid crystalline forms of CFZ; (c) ^{1}H-NMR spectra of the dissolved crystals.

3.2 Optical property assessment of CFZ

To assess the optical properties of CFZ, we first performed optical absorbance and photoacoustic spectroscopy measurements. Preliminary results show that photoacoustic signal intensity variations of different CFZ solutions are consistent with the optical absorbance spectra of CFZ. Fig. 5(a) shows that protonation results in a red-shift of the absorbance spectra with peaks at 450 nm, 495 nm and 540 nm for free-base CFZ (CFZ), monoprotonated CFZ (CFZ-H^+) and deprotonated CFZ (CFZ-$2H^+$), respectively.

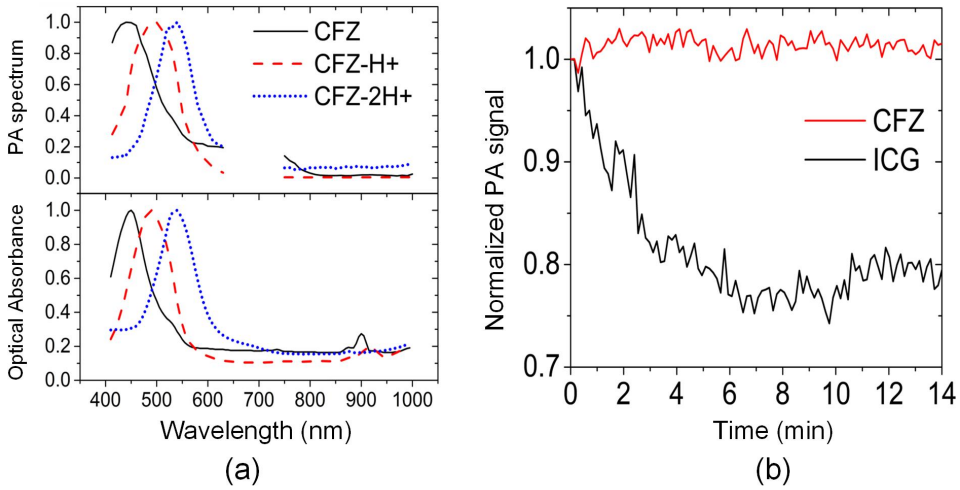

Fig. 5 Optical properties of CFZ. (a) Photoacosutic spectrum and optical absorbance of CFZ, CFZ-H+ and CFZ-2H+, (b) photostability of CFZ compared with ICG.

Downloaded From: http://proceedings.spiedigitallibrary.org/ on 03/25/2016 Terms of Use: http://spiedigitallibrary.org/ss/TermsOfUse.aspx

We also compared CFZ to another small molecule contrast agents, i.e. Indocyanine Green (ICG), which has strong absorbance at 800 nm [38] and is widely used for retinal angiography, liver function testing and cardiac output assessment. While ICG has a photoacoustic signal, it is also a photosensitizer. Comparing ICG and CFZ side-by-side [Fig. 5(b)] reveals that ICG bleaches very quickly upon laser illumination. Constant excitation of ICG with 750 nm light at 20 mJ/cm^2 (ANSI safety limit) results in ~25% decrease of photoacoustic signal amplitude within 6 minutes whereas CFZ appeared much more stable under the same conditions. The short *in vivo* half-life of ICG, typically less than five minutes, and its photosensitive toxicity, limits its potential application as a photoacoustic probe.

3.3 Clinically-relevant visualization of CFZ using the PA/US dual-modality system

For assaying photoacoustic signals of various CFZ formulations, phantoms were prepared using gelatin with four wells. Solubilized CFZ-H$^+$Cl$^-$, dissolved in DMSO at 10 mM and 5 mM concentrations, as well as CFZ-HCl particles (at 5 mM equivalent concentration) and CLDIs in aqueous buffer (also at 5 mM equivalent concentration) were injected into the wells. While solubilized CFZ-H$^+$Cl$^-$ in DMSO were bright red and homogenously transparent in color, the CFZ-HCl dispersion revealed CFZ forming dark aggregates. In contrast CLDIs remained well dispersed, leading to a deep red color. The US and PA results [Fig. 6(b) and 6(c)] reveal differences in the photoacoustic signal of CFZ at equivalent concentrations: CLDIs and CFZ-HCl (solid forms of the drug) had markedly stronger signal intensities than soluble CFZ in DMSO.

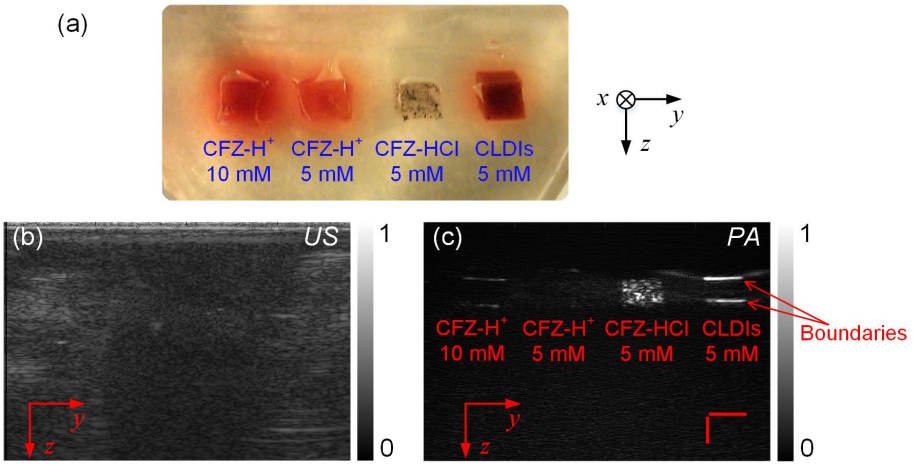

Fig. 6 PA/US dual-modality imaging of gelatin phantoms with different CFZ formulations. (a) Photograph of the gelatin phantom with embedded CFZ-H$^+$, CFZ-HCl and CLDIs, (b) US image and (c) PA image. Scale bar: 4 mm for both horizontal and vertical.

To demonstrate that CFZ can be imaged with a clinically-relevant, PA/US dual-modality setup, imaging experiments were also performed on a human cadaver index finger [Fig. 7(a)]. In the experiment, the metacarpophalangeal (MCP) joint in the index finger (largest joint amongst the human phalanges) was chosen as the site of the injection for solubilized CFZ-HCl. A syringe needle, guided by the PA/US dual-modality imaging system, was inserted in the targeted joint, about 5.6 mm beneath the skin surface [Fig. 7(b)]. CFZ was injected into the joint through the needle and the entire injection process lasted about 4 s, during which both PA and US images were continuously recorded. Pre- and post-injection PA and US results are shown in Fig. 7(c). In comparison with the image taken before the injection, the photoacoustic images taken after injection clearly show the presence and dispersion of CFZ (dashed rectangle) in the injected joint. Although the ultrasound images also show some signals during the injection, the contrast is low and the signals are not as strong as those in photoacoustic images, which give a much better visualization and understanding of the drug injecting process with optimum spatial diffusivity.

Downloaded From: http://proceedings.spiedigitallibrary.org/ on 03/25/2016 Terms of Use: http://spiedigitallibrary.org/ss/TermsOfUse.aspx

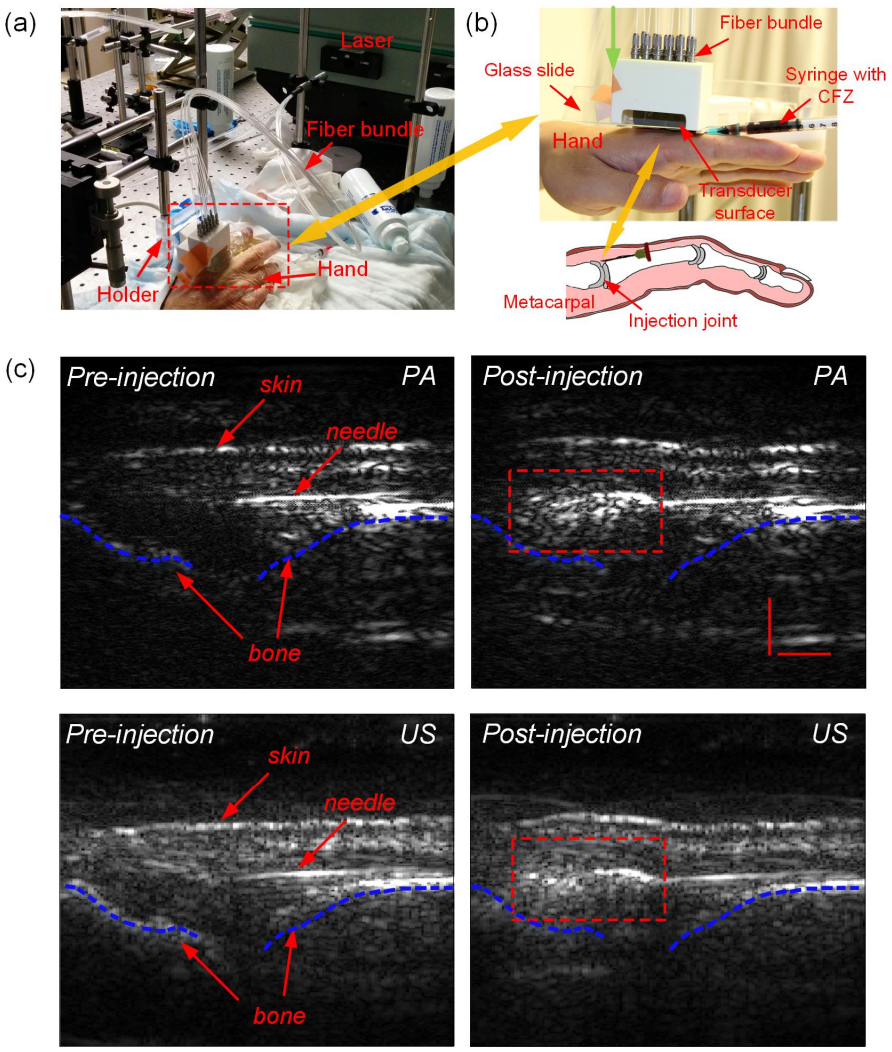

Fig. 7 Clinical visualization of CFZ injection into finger joints using the PA/US dual-modality system. (a) Experimental setup, (b) enlarged view of the imaging head and the injection joint, (c) PA and US images before and after the injection. Scale bar: 3 mm for both horizontal and vertical.

4. CONCLUSION

In summary, a PA/US dual modality imaging set up has been established, that allows us to visualize the distribution of the novel PAT contrast agent CFZ in the joints, in relation to the image obtained by the US imaging system. CFZ can be formulated in a variety of salt forms, which can mimic (more or less) the natural inclusions formed by CFZ in mammalian organisms, leading to various new kinds of contrast agent formulations with potentially useful optical properties for functional imaging experiments. The potential clinical utility of the dual PA/US imaging system was demonstrated with gelatin phantoms and a human cadaver experiments. The experimental results reveal that the PA/US imaging set up could be clinical useful, in terms of the diagnosis and image guided therapy of arthritis.

ACKNOWLEDGEMENTS

This work was supported by National Institutes of Health (NIH) under grant numbers R01GM078200, R01AR060350 and R01CA186769.

Downloaded From: http://proceedings.spiedigitallibrary.org/ on 03/25/2016 Terms of Use: http://spiedigitallibrary.org/ss/TermsOfUse.aspx

REFERENCES

[1] P. Jacobs, R. Bissonnette, and L. C. Guenther, "Socioeconomic burden of immune-mediated inflammatory diseases-focusing on work productivity and disability," The Journal of Rheumatology **88**, 55-61 (2011).

[2] A. Boonen and W. Mau, "The economic burden of disease: comparison between rheumatoid arthritis and ankylosing spondylitis," Clinical & Experimental Rheumatology **27**, S112 (2009).

[3] D. Chamberland, Y. Jiang, and X. Wang, "Optical imaging: new tools for arthritis," Integrative Biology **2**, 496-509 (2010).

[4] M. Østergaard, B. Ejbjerg, and M. Szkudlarek, "Imaging in early rheumatoid arthritis: roles of magnetic resonance imaging, ultrasonography, conventional radiography and computed tomography," Best Practice & Research Clinical Rheumatology **19**, 91-116 (2005).

[5] C. Tian, Z. Xie, M. L. Fabiilli, and X. Wang, "Imaging and sensing based on dual-pulse nonlinear photoacoustic contrast: a preliminary study on fatty liver," Opt. Lett. **40**, 2253-2256 (2015).

[6] C. Tian, Z. Xie, M. L. Fabiilli, S. Liu, C. Wang, Q. Cheng, and X. Wang, "Dual-pulse nonlinear photoacoustic technique: a practical investigation," Biomed. Opt. Express **6**, 2923-2933 (2015).

[7] T. Feng, K. M. Kozloff, C. Tian, J. E. Perosky, Y.-S. Hsiao, S. Du, J. Yuan, C. X. Deng, and X. Wang, "Bone assessment via thermal photo-acoustic measurements," Opt. Lett. **40**, 1721-1724 (2015).

[8] T. Feng, J. E. Perosky, K. M. Kozloff, G. Xu, Q. Cheng, S. Du, J. Yuan, C. X. Deng, and X. Wang, "Characterization of bone microstructure using photoacoustic spectrum analysis," Opt. Express **23**, 25217-25224 (2015).

[9] Z. Xie, C. Tian, S.-L. Chen, T. Ling, C. Zhang, L. J. Guo, P. L. Carson, and X. Wang, "3D high resolution photoacoustic imaging based on pure optical photoacoustic microscopy with microring resonator," in *SPIE BiOS*, (International Society for Optics and Photonics, 2014), 894314-894314-894316.

[10] G. Xu, J. R. Rajian, G. Girish, M. J. Kaplan, J. B. Fowlkes, P. L. Carson, and X. Wang, "Photoacoustic and ultrasound dual-modality imaging of human peripheral joints," Journal of biomedical optics **18**, 010502-010502 (2013).

[11] J. R. Rajian, G. Girish, and X. Wang, "Photoacoustic tomography to identify inflammatory arthritis," Journal of biomedical optics **17**, 0960131-0960136 (2012).

[12] N. Beziere, C. Schacky, Y. Kosanke, M. Kimm, A. Nunes, K. Licha, M. Aichler, A. Walch, E. Rummeny, and V. Ntziachristos, "Optoacoustic imaging and staging of inflammation in a murine model of arthritis," Arthritis & Rheumatology **66**, 2071-2078 (2014).

[13] R. K. Keswani, C. Tian, T. Peryea, G. Gandikota, X. Wang, and G. R. Rosania, "Repositioning Clofazimine as a Clinical Macrophage-Targeting Photoacoustic Contrast Agent," Sci. Rep. (2016). under revision

[14] D. L. Chamberland, A. Agarwal, N. Kotov, J. B. Fowlkes, P. L. Carson, and X. Wang, "Photoacoustic tomography of joints aided by an Etanercept-conjugated gold nanoparticle contrast agent—an ex vivo preliminary rat study," Nanotechnology **19**, 095101 (2008).

[15] V. C. Barry, J. Belton, M. L. Conalty, J. M. Denneny, D. W. Edward, J. O'sullivan, D. Twomey, and F. Winder, "A new series of phenazines (rimino-compounds) with high antituberculosis activity," Nature **179**, 1013-1015 (1957).

[16] Y. Lu, M. Zheng, B. Wang, L. Fu, W. Zhao, P. Li, J. Xu, H. Zhu, H. Jin, and D. Yin, "Clofazimine analogs with efficacy against experimental tuberculosis and reduced potential for accumulation," Antimicrobial agents and chemotherapy **55**, 5185-5193 (2011).

[17] V. M. Reddy, J. F. O'Sullivan, and P. R. Gangadharam, "Antimycobacterial activities of riminophenazines," Journal of Antimicrobial Chemotherapy **43**, 615-623 (1999).

[18] L. Levy, "Pharmacologic studies of clofazimine," The American journal of tropical medicine and hygiene **23**, 1097-1109 (1974).

[19] M. C. Cholo, H. C. Steel, P. B. Fourie, W. A. Germishuizen, and R. Anderson, "Clofazimine: current status and future prospects," Journal of antimicrobial chemotherapy, dkr444 (2011).

[20] J. L. Arbiser and S. L. Moschella, "Clofazimine: a review of its medical uses and mechanisms of action," Journal of the American Academy of Dermatology **32**, 241-247 (1995).

[21] J. C. Garrelts, "Clofazimine: a review of its use in leprosy and Mycobacterium avium complex infection," Annals of Pharmacotherapy **25**, 525-531 (1991).

[22] D. P. Legendre, C. A. Muzny, and E. Swiatlo, "Hansen's Disease (Leprosy): Current and Future Pharmacotherapy and Treatment of Disease-Related Immunologic Reactions," Pharmacotherapy: The Journal of Human Pharmacology and Drug Therapy **32**, 27-37 (2012).

Downloaded From: http://proceedings.spiedigitallibrary.org/ on 03/25/2016 Terms of Use: http://spiedigitallibrary.org/ss/TermsOfUse.aspx

[23] M. L. Conalty, V. C. Barry, and A. Jina, "The antileprosy agent B. 663 (Clofazimine) and the reticuloendothelial system," Int J Lepr Other Mycobact Dis **39**, 479-492 (1971).
[24] R. H. C. QUEIROZ, A. M. de SOUZA, S. V. Sampaio, and E. Melchior, "Biochemical and hematological side effects of clofazimine in leprosy patients," Pharmacological research **46**, 191-194 (2002).
[25] S. Sukpanichnant, N. S. Hargrove, U. Kachintorn, S. Manatsathit, T. Chanchairujira, N. Siritanaratkul, T. Akaraviputh, and K. Thakerngpol, "Clofazimine-induced crystal-storing histiocytosis producing chronic abdominal pain in a leprosy patient," The American journal of surgical pathology **24**, 129 (2000).
[26] J. Baik, K. A. Stringer, G. Mane, and G. R. Rosania, "Multiscale distribution and bioaccumulation analysis of clofazimine reveals a massive immune system-mediated xenobiotic sequestration response," Antimicrobial agents and chemotherapy **57**, 1218-1230 (2013).
[27] J. Baik and G. R. Rosania, "Macrophages sequester clofazimine in an intracellular liquid crystal-like supramolecular organization," (2012).
[28] A. McDougall, "Electron microscope studies of the antileprosy drug B663 (clofazimine; Lamprenel)," International journal of leprosy and other mycobacterial diseases: official organ of the International Leprosy Association **42**, 1 (1974).
[29] R. K. Keswani, J. Baik, L. Yeomans, C. Hitzman, A. Johnson, A. Pawate, P. J. Kenis, N. Rodríguez-Hornedo, K. A. Stringer, and G. R. Rosania, "Chemical Analysis of Drug Biocrystals: A Role for Counterion Transport Pathways in Intracellular Drug Disposition," Molecular pharmaceutics (2015).
[30] E. L. M. Bezerra, M. J. P. Vilar, P. B. da Trindade Neto, and I. Sato, "Double-blind, randomized, controlled clinical trial of clofazimine compared with chloroquine in patients with systemic lupus erythematosus," Arthritis & Rheumatism **52**, 3073-3078 (2005).
[31] J. Mackey and J. Barnes, "Clofazimine in the treatment of discoid lupus erythematosus," British Journal of Dermatology **91**, 93-96 (1974).
[32] G. S. Yoon, S. Sud, R. K. Keswani, J. Baik, T. J. Standiford, K. A. Stringer, and G. R. Rosania, "Phagocytosed Clofazimine Biocrystals can Modulate Innate Immune Signaling by Inhibiting TNFα and Boosting IL-1RA Secretion," Molecular pharmaceutics (2015).
[33] L. B. Adams, I. Sinha, S. G. Franzblau, J. L. Krahenbuhl, and R. T. Mehta, "Effective treatment of acute and chronic murine tuberculosis with liposome-encapsulated clofazimine," Antimicrobial agents and chemotherapy **43**, 1638-1643 (1999).
[34] R. T. Mehta, A. Keyhani, T. J. McQueen, B. Rosenbaum, K. V. Rolston, and J. J. Tarrand, "In vitro activities of free and liposomal drugs against Mycobacterium avium-M. intracellulare complex and M. tuberculosis," Antimicrobial agents and chemotherapy **37**, 2584-2587 (1993).
[35] C.-G. Park, N. W. Thiex, K.-M. Lee, G. L. Szot, J. A. Bluestone, and K.-D. Lee, "Targeting and blocking B7 costimulatory molecules on antigen-presenting cells using CTLA4Ig-conjugated liposomes: in vitro characterization and in vivo factors affecting biodistribution," Pharmaceutical research **20**, 1239-1248 (2003).
[36] K. Peters, S. Leitzke, J. Diederichs, K. Borner, H. Hahn, R. Müller, and S. Ehlers, "Preparation of a clofazimine nanosuspension for intravenous use and evaluation of its therapeutic efficacy in murine Mycobacterium avium infection," Journal of Antimicrobial Chemotherapy **45**, 77-83 (2000).
[37] R. K. Keswani, G. S. Yoon, S. Sud, K. A. Stringer, and G. R. Rosania, "A far-red fluorescent probe for flow cytometry and image-based functional studies of xenobiotic sequestering macrophages," Cytometry Part A **87**, 855-867 (2015).
[38] S. Prahl, "Optical Absorption of Indocyanine Green (ICG)", retrieved 01/17, 2016, http://omlc.org/spectra/icg/index.html.

Downloaded From: http://proceedings.spiedigitallibrary.org/ on 03/25/2016 Terms of Use: http://spiedigitallibrary.org/ss/TermsOfUse.aspx